each of the cases depicted in Fig. 4A and observed that as γ_{tip} was increased, the $P_{Raman\text{-}threshold}$ increased at first but then decreased (Fig. 4B).

These observations are in stark contrast with what one would expect in conventional systems, where the higher the loss, the higher the lasing threshold. Surprisingly, in the vicinity of an EP, less loss is detrimental and annihilates the process of interest; more loss is good because it helps to recover the process. This counterintuitive effect happens because the supermodes of the coupled system readjust themselves as loss is gradually increased. When the loss exceeds a critical value, one supermode is mostly located in the subsystem with less loss and, thus, the total field can build up more strongly (*20*). As our results demonstrate, this behavior also affects nonlinear processes, such as thermal broadening and Raman lasing, that rely on intracavity field intensity.

Our system provides a comprehensive platform for further studies of EPs and opens up new avenues of research on non-Hermitian systems and their behavior. Our findings may also lead to new schemes and techniques for controlling and reversing the effects of loss in other physical systems, such as in photonic crystal cavities, plasmonic structures, and metamaterials.

REFERENCES AND NOTES

1. C. M. Bender, *Rep. Prog. Phys.* **70**, 947–1018 (2007).
2. I. Rotter, *J. Phys. Math. Theor.* **42**, 153001 (2009).
3. N. Moiseyev, *Non-Hermitian Quantum Mechanics* (Cambridge Univ. Press, Cambridge, 2011).
4. W. D. Heiss, *J. Phys. A* **37**, 2455–2464 (2004).
5. E. Persson, I. Rotter, H. Stöckmann, M. Barth, *Phys. Rev. Lett.* **85**, 2478–2481 (2000).
6. C. Dembowski *et al.*, *Phys. Rev. Lett.* **86**, 787–790 (2001).
7. S. B. Lee *et al.*, *Phys. Rev. Lett.* **103**, 134101 (2009).
8. C. M. Bender, S. Boettcher, *Phys. Rev. Lett.* **80**, 5243–5246 (1998).
9. R. El-Ganainy, K. G. Makris, D. N. Christodoulides, Z. H. Musslimani, *Opt. Lett.* **32**, 2632–2634 (2007).
10. C. E. Rüter *et al.*, *Nat. Phys.* **6**, 192–195 (2010).
11. A. Guo *et al.*, *Phys. Rev. Lett.* **103**, 093902 (2009).
12. A. Regensburger *et al.*, *Nature* **488**, 167–171 (2012).
13. L. Feng *et al.*, *Nat. Mater.* **12**, 108–113 (2013).
14. L. Feng *et al.*, *Opt. Express* **22**, 1760–1767 (2014).
15. H. Wenzel, U. Bandelow, H.-J. Wünsche, J. Rehberg, *IEEE J. Quantum Electron.* **32**, 69–78 (1996).
16. M. V. Berry, *J. Mod. Opt.* **50**, 63–81 (2003).
17. M. Liertzer *et al.*, *Phys. Rev. Lett.* **108**, 173901 (2012).
18. B. Peng *et al.*, *Nat. Phys.* **10**, 394–398 (2014).
19. M. Brandstetter *et al.*, *Nat. Commun.* **5**, 4034 (2014).
20. Supplementary materials are available on *Science* Online.
21. K. J. Vahala, *Nature* **424**, 839–846 (2003).
22. D. O'Shea, C. Junge, J. Volz, A. Rauschenbeutel, *Phys. Rev. Lett.* **111**, 193601 (2013).
23. T. J. Kippenberg, K. J. Vahala, *Science* **321**, 1172–1176 (2008).
24. L. He, S. K. Ozdemir, L. Yang, *Laser & Photon. Rev.* **7**, 60–82 (2013).
25. X. Fan *et al.*, *Anal. Chim. Acta* **620**, 8–26 (2008).
26. F. Vollmer, S. Arnold, *Nat. Methods* **5**, 591–596 (2008).
27. J. Zhu *et al.*, *Nat. Photonics* **4**, 46–49 (2010).
28. T. Carmon, L. Yang, K. Vahala, *Opt. Express* **12**, 4742–4750 (2004).
29. S. M. Spillane, T. J. Kippenberg, K. J. Vahala, *Nature* **415**, 621–623 (2002).
30. S. K. Ozdemir *et al.*, *Proc. Natl. Acad. Sci. U.S.A.* **111**, E3836–E3844 (2014).

ACKNOWLEDGMENTS

Ş.K.O. and L.Y. conceived the idea and designed the experiments. B.P. and Ş.K.O. performed the experiments with help from H.Y. and F.M. Theoretical background and simulations were provided by B.P., Ş.K.O., S.R., M.L., C.M.B., and F.N. All authors discussed the results, and Ş.K.O., S.R., and L.Y. wrote the manuscript with input from all authors. This work was supported by Army Research Office (ARO) grant no. W911NF-12-1-0026. C.M.B. was supported by U.S. Department of Energy grant no. DE-FG02-91ER40628. F.N. is partially supported by the RIKEN iTHES Project, Multidisciplinary University Research Initiatives (MURI) Center for Dynamic Magneto-Optics, Grant-in-Aid for Scientific Research (S). S.R. and M.L. are supported by the Vienna Science and Technology Fund (WWTF) project no. MA09-030 and by the Austrian Science Fund (FWF) project no. SFB-IR-ON F25-P14, SFB-NextLite F49-P10.

SUPPLEMENTARY MATERIALS

www.sciencemag.org/content/346/6207/328/suppl/DC1
Supplementary Text
Figs. S1 to S16
Table S1
References (*31*–*34*)

27 June 2014; accepted 11 September 2014
10.1126/science.1258004

QUANTUM ELECTRONICS

Cavity quantum electrodynamics with many-body states of a two-dimensional electron gas

Stephan Smolka,[1]* Wolf Wuester,[1,2]* Florian Haupt,[1] Stefan Faelt,[1,2] Werner Wegscheider,[2] Ataç Imamoglu[1]†

Light-matter interaction has played a central role in understanding as well as engineering new states of matter. Reversible coupling of excitons and photons enabled groundbreaking results in condensation and superfluidity of nonequilibrium quasiparticles with a photonic component. We investigated such cavity-polaritons in the presence of a high-mobility two-dimensional electron gas, exhibiting strongly correlated phases. When the cavity was on resonance with the Fermi level, we observed previously unknown many-body physics associated with a dynamical hole-scattering potential. In finite magnetic fields, polaritons show distinct signatures of integer and fractional quantum Hall ground states. Our results lay the groundwork for probing nonequilibrium dynamics of quantum Hall states and exploiting the electron density dependence of polariton splitting so as to obtain ultrastrong optical nonlinearities.

Strong electric-dipole coupling of excitons in an intrinsic semiconductor quantum well (QW) to microcavity photons leads to the formation of mixed light-matter quasiparticles called cavity-polaritons (*1*, *2*). In contrast to excitons, optical excitations from a two-dimensional electron gas (2DEG) show many-body effects associated with the abrupt turn-on of a valence-band hole-scattering potential. The resulting absorption spectrum exhibits a power-law divergence, stemming from final-state interaction effects that lead to orthogonal initial and final many-body wave functions, and is referred to as Fermi-edge singularity (*3*). Despite initial attempts (*4*–*6*), the nature of strong coupling of a Fermi-edge singularity, rather than an exciton, to a microcavity mode remained largely unexplored.

We investigated a 2DEG in a modulation-doped GaAs QW embedded in a distributed Bragg reflector (DBR) microcavity (Fig. 1A). We used this system to analyze two distinct problems: In the absence of an external magnetic field (B_z = 0), optical excitations from a 2DEG are simultaneously subject to Coulomb interactions and strong cavity coupling, which lead to the formation of Fermi-edge polaritons—a many-body excitation with a dynamical valence-hole scattering potential (*7*). In the $B_z \neq 0$ limit, we establish cavity quantum electrodynamics (QED) as a new paradigm for investigating integer and fractional quantum Hall (QH) states (*8*) in which information about a strongly correlated electronic ground state is transcribed onto the reflection and transmission amplitudes of a single-cavity photon.

The dispersion of the relevant electronic states when B_z = 0 is shown in Fig. 1B, left. The Fermi energy E_F is tuned by applying a gate voltage (V_g) between a p-doped GaAs top layer and the 2DEG. When $B_z \neq 0$, the electronic states form discrete Landau levels (LLs) (Fig. 1B, right). Each (spin-resolved) LL has a degeneracy $e\,B_z/h$; the filling factor $\nu = n_e\,h/(e\,B_z)$ determines the number of filled LLs at a given electron density n_e. We studied two different samples with gate-tunable n_e: sample *A* exhibits an electron mobility of $\mu = 2 \times 10^5$ cm^2(V s)$^{-1}$ at $n_e = 1.0 \times 10^{11}$ cm^{-2} (*9*). Sample *B* exhibits an order-of-magnitude-higher mobility of $\mu = 2.5 \times 10^6$ cm^2(V s)$^{-1}$ at $n_e = 2.3 \times 10^{11}$ cm^{-2}.

The differential reflectivity (dR) (*9*) spectra of sample *A* (blue) is shown in Fig. 1D as the electron density n_e in the 2DEG is varied from $n_e < 2 \times 10^{10}$ cm^{-2} to $n_e = 8 \times 10^{10}$ cm^{-2}. The cavity mode is visible as a dR peak at 1521 meV. Changing n_e modifies the nature of elementary optical excitations: At low electron densities

[1]Institute of Quantum Electronics, Eidgenössische Technische Hochschule (ETH) Zurich, 8093 Zurich, Switzerland. [2]Solid State Physics Laboratory, ETH Zurich, 8093 Zurich, Switzerland.
*These authors contributed equally to this work. †Corresponding author. E-mail: imamoglu@phys.ethz.ch

($n_e < 2 \times 10^{10}$ cm^{-2}), the QW spectrum is dominated by the heavy-hole exciton X^0_{hh} peak. The weak resonance on the red side of X^0_{hh} stems from the excitation of a bound state of two electrons and one hole (X^-, trion). For 2×10^{10} cm$^{-2} \leq n_e < 8 \times 10^{10}$ cm^{-2}, the trion transition emerges as the dominant feature in the spectrum. Increasing n_e leads to an asymmetry in the X^- line shape and a blue-shift of its center frequency (*10*). Last, for $n_e > 8 \times 10^{10}$ cm^{-2} the absorption spectrum is dominated by an asymmetric resonance at the Fermi edge (*11*). Photoluminescence (PL) spectra, obtained after tuning the cavity mode to 1531 meV, is shown with dR in Fig. 1D in orange. For $n_e > 6 \times 10^{10}$ cm^{-2}, the PL spectrum (*12*) exhibits a double-peaked structure with a total width that agrees well with E_F, which was estimated by using independently determined n_e (*9*).

We first address the confluence of Fermi-edge singularity and nonperturbative light-matter coupling (Fig. 2). In stark contrast to earlier work on edge singularity physics, our system exhibits a dynamical hole-scattering potential due to vacuum Rabi oscillations in the final state of the optical transition, and a finite hole recoil induced modification of the cavity-2DEG coupling. Prior work—based on a fixed n_e 2DEG embedded in a microcavity—demonstrated normal-mode splitting at a relatively high temperature of 2 K and used single-particle transfer-matrix calculations to obtain a fit to the data (*5*). However, we show that only by measuring the polariton dispersion as well as the n_e, mobility, and temperature dependence of the vacuum Rabi coupling is it possible to develop a consistent picture of the underlying many-body physics.

To demonstrate nonperturbative light-matter coupling, we fixed n_e to 1.2×10^{11} cm^{-2} in sample *A* and tuned the cavity mode across the absorption edge at E_F. When the cavity frequency E_c is resonant with E_F (Fig. 2A), we observe normal-mode splitting of $2g = (2.0 \pm 0.1)$ meV, with g denoting the dipole-coupling strength. Because $2g$ is larger than the bare-cavity linewidth $\Gamma_c = 1$ meV, it is concluded that the system is in the strong coupling regime of cavity-QED, where the elementary optical excitations could be described as trion/Fermi-edge polaritons (*5*, *13*). In contrast to the exciton-polariton excitations observed in undoped QWs coupled to microcavities (*1*), in our case the upper polariton is substantially broader than the lower polariton. This broadening and the asymmetry stem from the shake-up of the Fermi sea that accompanies bound-trion or Fermi-edge resonance formation (*6*).

The dispersion of Fermi-edge polaritons is shown in Fig. 2B. The data were obtained by measuring angle-resolved dR spectra (*14*) for a cavity detuning that yields minimal normal-mode splitting at normal incidence (Fig. 2A). We observed two split branches, each with an ultra-small effective polariton mass, which is approximately twice as large as that of the bare cavity-photon mass (*9*).

In order to study the density and mobility dependence of the Fermi-edge polaritons, we recorded the polariton excitations versus detuning from the Fermi edge at $n_e = 1.6 \times 10^{11}$ cm^{-2} on the high-mobility sample *B* (Fig. 2C). The data shows a significantly smaller normal-mode splitting as compared with that of sample *A* (Fig. 2A), which is a consequence of weaker hole confinement owing to higher n_e and mobility. A detailed study of the normal-mode splitting at resonance as a function of n_e is presented in Fig. 2D, showing a clear decrease from $2g = (2.0 \pm 0.1)$ meV to $2g = (1.3 \pm 0.2)$ meV as the density is increased from $n_e = 0.8 \times 10^{11}$ cm^{-2} to $n_e = 1.6 \times 10^{11}$ cm^{-2} (*9*). The scattering of an electron with momentum $\sim k_F$ on the Fermi surface is accompanied by a hole momentum kick, leading to a hole recoil energy E_r (*15*). A larger hole recoil partially inhibits the formation of the electron screening cloud as $n_e(k_F)$ is increased, resulting in the observed reduction of the normal-mode splitting.

Remarkably, polariton excitations depend strongly on temperature as well. When we compare the $n_e = 0.9 \times 10^{11}$ cm^{-2} dR spectrum at $T = 0.2$ K with the one at $T = 4$ K (Fig. 2D, inset), we observe that the normal-mode splitting disappears at $T = 4$ K. This observation is striking because the corresponding splitting at $T = 0.2$ K ($2g = 1.3 \pm 0.2$ meV) is larger than the thermal energy $E_T = 345$ μeV at $T = 4$ K.

Our experimental findings point to a scenario in which the nonperturbative cavity-QW coupling leads to the formation of Fermi-edge polaritons for $n_e > 8 \times 10^{10}$ cm^{-2}. In contrast to the Fermi-edge singularity associated with screening of a localized hole by the Fermi sea (*4*, *6*), these new many-body optical excitations are delocalized as demonstrated by the polariton dispersion (Fig. 2B). A key requirement for the observation of Fermi-edge polaritons is that the cavity-QW coupling strength exceeds E_r: in this limit, the enhancement of the 2DEG-cavity coupling by optical excitations with energy $\geq E_F + E_r$ ensures strong coupling, albeit with reduced normal-mode splitting. This conclusion is supported by the reduction of normal-mode splitting (Fig. 2D) with increasing n_e, or equivalently, increasing E_r observed in the high-mobility

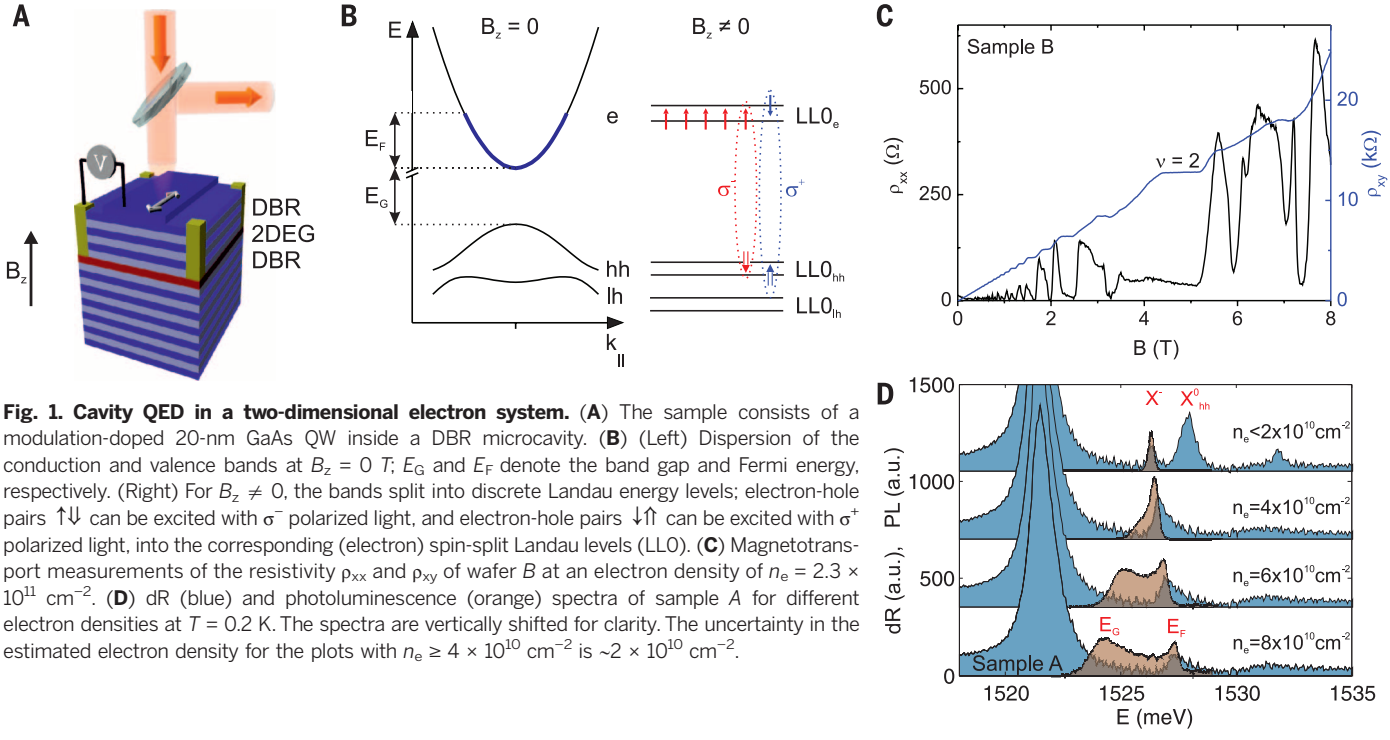

Fig. 1. Cavity QED in a two-dimensional electron system. (**A**) The sample consists of a modulation-doped 20-nm GaAs QW inside a DBR microcavity. (**B**) (Left) Dispersion of the conduction and valence bands at $B_z = 0$ *T*; E_G and E_F denote the band gap and Fermi energy, respectively. (Right) For $B_z \neq 0$, the bands split into discrete Landau energy levels; electron-hole pairs ↑⇓ can be excited with σ^- polarized light, and electron-hole pairs ↓⇑ can be excited with σ^+ polarized light, into the corresponding (electron) spin-split Landau levels (LL0). (**C**) Magnetotransport measurements of the resistivity ρ_{xx} and ρ_{xy} of wafer *B* at an electron density of $n_e = 2.3 \times 10^{11}$ cm^{-2}. (**D**) dR (blue) and photoluminescence (orange) spectra of sample *A* for different electron densities at $T = 0.2$ K. The spectra are vertically shifted for clarity. The uncertainty in the estimated electron density for the plots with $n_e \geq 4 \times 10^{10}$ cm^{-2} is ~2×10^{10} cm^{-2}.

sample *B*. Conversely, the persistence of polariton splitting implies that the hole population in the QW exhibits Rabi oscillations, leading to a time-dependent scattering potential.

In contrast to the $B_z = 0$ limit at which the initial state of the optical transition is a Fermi sea without interaction-induced correlations, the electronic states for $B_z \neq 0$ in the absence of photonic excitations are QH states. We analyzed polariton excitations out of these many-body states by performing polarization-resolved dR measurements. Because the absorption of right-hand circularly polarized σ^+ light generates a spin-down $|\downarrow\rangle$ electron and a $|\Uparrow\rangle$ heavy-hole, and absorption of left-hand circularly polarized σ^- light generates a spin-up $|\uparrow\rangle$ electron and a $|\Downarrow\rangle$ heavy-hole, the observed spectrum is highly sensitive to spin polarization-dependent phase-space-filling. When the magnetic field is increased, the filling factor ν is reduced, allowing optical absorption into LLs that are no longer (completely) filled. In Fig. 3, A and B, the cavity resonance on sample *B* is tuned to $E = 1523.8$ meV. In the low field range ($B_z = 0 - 2$ T), absorption into higher lying empty LLs ($\nu \geq 2$), enabled by the weak off-resonant coupling of these resonances to the cavity mode, is visible.

The reflection spectrum from the lowest LL (LL0) at $n_e = 1.4 \times 10^{11}$ cm^{-2} (Fig. 3, A and B) shows that a finite polariton splitting emerges at $B_z \sim 3$ T ($\nu \sim 2$). To study the resonant interaction between the cavity mode and the optical excitations of QH states, we fixed $B_z = 3$ T, tuned the cavity to resonance with the LL0 spin-up (σ^-) transition at $\nu = 2$, and varied n_e through V_g. For both light polarizations, only the bare cavity resonance is visible for $\nu \geq 2$ because phase-space-filling blocks all 2DEG optical excitations at E_c (Fig. 3, C and D). In contrast, a normal-mode splitting appears for $\nu < 2$; the splitting grows monotonically as n_e is reduced because the number of available final states is thereby increased. The normal-mode splitting of σ^+ polarization starts at higher ν than the one of σ^-, suggesting that 2DEG electrons remain spin-polarized for $1.7 \leq \nu < 2.0$.

Unlike the $B_z = 0$ case, the normal-mode splitting at $B_z \neq 0$ is comparable with that of a heavy-hole exciton polariton in the limit $n_e \rightarrow 0$, pointing to a reduced screening of electron-hole attraction. The dominant optical excitations into LL0 for $1 < \nu < 2$ can be described as heavy-hole singlet trions (*16*) because the strongest binding energy and the highest optical oscillator strength would be obtained for a complex of two electrons of opposite spin in the same electronic orbital m of size $\cong a_m = \sqrt{\hbar/eB_z}$ and a heavy-hole with a strong spatial overlap. Such a trion could have an absorption strength comparable with that obtained for an exciton because the magnetic length a_m is comparable with the exciton Bohr radius for $B_z \sim 5$T.

By increasing the magnetic field to $B_z = 4.9$ T, we explored polariton excitations around $\nu = 1$. In Fig. 3, E and F, we see a drastic change in the optical response: Whereas the normal-mode splitting collapses for σ^- light, it increases sharply for σ^+. This feature shows the emergence of a high degree of spin polarization, which we associate with the $\nu = 1$ integer QH state (*17*, *18*). In case of full spin polarization, the oscillator strength ($\propto g^2$) of the σ^+ polariton excitations is maximum because no $|\downarrow\rangle$ states are occupied. For $\nu = 1$, the degree of spin polarization, $P = (g^2_{\sigma^+} - g^2_{\sigma^-})/(g^2_{\sigma^+} + g^2_{\sigma^-})$, is determined from the measured minimum normal-mode splittings and found to be $P = 90 \pm 10\%$. The error arises primarily from the measurement uncertainty of the individual splittings and simultaneous coupling to higher lying optical transitions. As we moved away to both sides from $\nu = 1$ by changing either V_g or B_z, we observed a symmetric decrease of the normal-mode splitting for the σ^- polariton excitations and a symmetric increase of the normal-mode splitting for the σ^+ polariton excitations, which we attribute to spin-depolarization due to skyrmion excitations (*19*).

In order to investigate fractional QH states, we tuned E_c into resonance with the $|\downarrow\rangle$-transition of LL0 at $\nu = 2/3$. dR spectra at $B_z = 6$ T as a function of n_e is presented in Fig. 4, A and B. For $\nu \cong 2/3$, we observed a small decrease in the normal-mode splitting for the σ^- polariton modes and a small increase in the normal-mode splitting for the σ^+ polariton modes, which points to enhanced spin polarization associated with the $\nu = 2/3$ fractional QH state (*20*, *21*). The small change in the splitting stems from the sizeable degree of spin polarization that persists for $\forall \nu < 1$ and the fact that even for complete spin polarization at $\nu = 2/3$, one third of the states in the spin-up LL0 are available for excitonic excitations. To highlight the variations in the normal-mode splitting, we plot in Fig. 4C the energy difference ΔE_{LP} between the dR peaks of the σ^+ and σ^- lower polariton branches as a function of ν at $B_z = 6$ T (blue circles): A local maximum in ΔE_{LP} around the fractional QH state $\nu = 2/3$ signifies spin polarization (*22*–*25*). To confirm that the peak in ΔE_{LP} at $\nu = 2/3$ does not have an auxiliary origin, we spatially tuned the cavity mode to $E_{\nu=1}$ (Fig. 4C, red squares) and found that the local maximum in ΔE_{LP} at $\nu = 2/3$ persists.

It has been previously established that a phase transition from an unpolarized $\nu = 2/3$ to a polarized $\nu = 2/3$ QH ground state takes place at a critical magnetic field B_c that depends strongly on the effective width of the electron wave function (*26*, *27*). At a lower magnetic field of $B_z = 4.9$ T (Figs. 3, E and F), we did not observe a local maximum in ΔE_{LP} at $\nu = 2/3$ (Fig. 4C), suggesting that the excess spin polarization is lost; this observation is consistent with a phase transition from an unpolarized to a polarized $\nu = 2/3$ state.

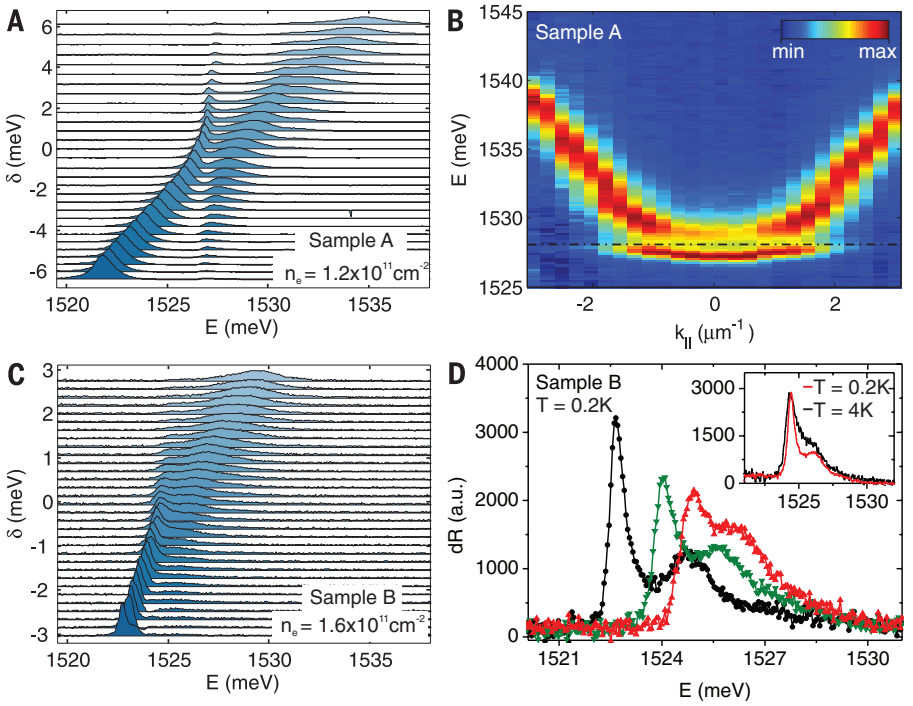

Fig. 2. Experimental signatures of Fermi-edge polaritons. (**A**) dR spectra taken from sample *A* as a function of cavity detuning δ from the Fermi edge at $T = 0.2$ K and $n_e = 1.2 \times 10^{11}$ cm^{-2}. (**B**) Fermi-edge polariton energy dispersion obtained at $T = 1.6$ K, $n_e = 1.2 \times 10^{11}$ cm^{-2}, and $\delta = 0$. The dashed straight line depicts the Fermi energy. The blue color-coded area displays low dR signal, and the red color-coded area displays high dR signal. (**C**) dR spectra measured on sample *B* versus cavity detuning at $T = 0.2$ K and $n_e = 1.6 \times 10^{11}$ cm^{-2}. (**D**) dR spectra for different densities from sample *B* at $\delta = 0$ and $T = 0.2$ K for $n_e = 0.8 \times 10^{11}$ cm^{-2} (black), $n_e = 1.2 \times 10^{11}$ cm^{-2} (green), and $n_e = 1.6 \times 10^{11}$ cm^{-2} (red). The spectra shift to higher energies as the density increases due to the increasing E_F. (Inset) dR spectra for two different temperatures of $T = 0.2$ K (red) and $T = 4$ K (black) at $\delta = 0$. In both cases, we have $n_e = 0.9 \times 10^{11}$ cm^{-2}.

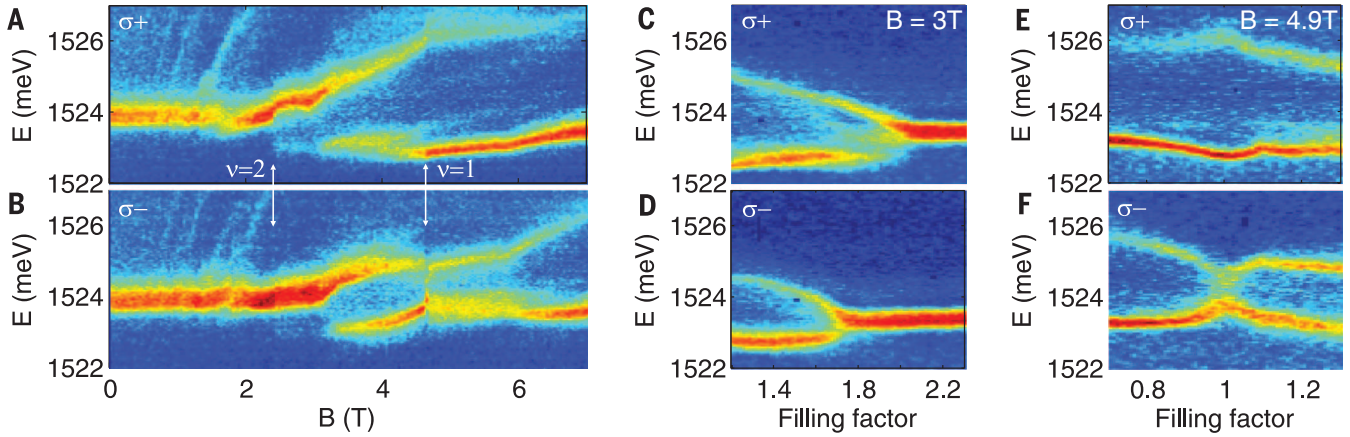

Fig. 3. Integer QH polariton excitations. (**A** and **B**) Polarization-resolved dR measurements versus magnetic field of sample *B* at a constant cavity energy of E_c = 1523.8 meV and an electron density of $n_e = 1.4 \times 10^{11}$ cm^{-2} (V_g = −4 V). (**C** and **D**) Polarization-resolved dR measurements versus V_g around ν = 2 when the cavity energy is on resonance with the lowest Landau level (B_z = 3 T). The blue color-code represents low dR signal, and the red color-code represents high dR signal. σ^+ corresponds to right-hand circularly polarized light, and σ^- corresponds to left-hand circularly polarized light. (**E** and **F**) Polarization-resolved dR measurements as a function of the filling factor obtained by changing V_g around ν = 1 at a magnetic field of B_z = 4.9 T for σ^+- in (E) and σ^--polarized light in (F). The spectral white light power in (A) and (B) is $P \approx 15$ pW nm^{-1}. In (C) to (F), we used a spectral power $P \approx 0.2$ pW nm^{-1}; the plotted data are an average over 150 measurements.

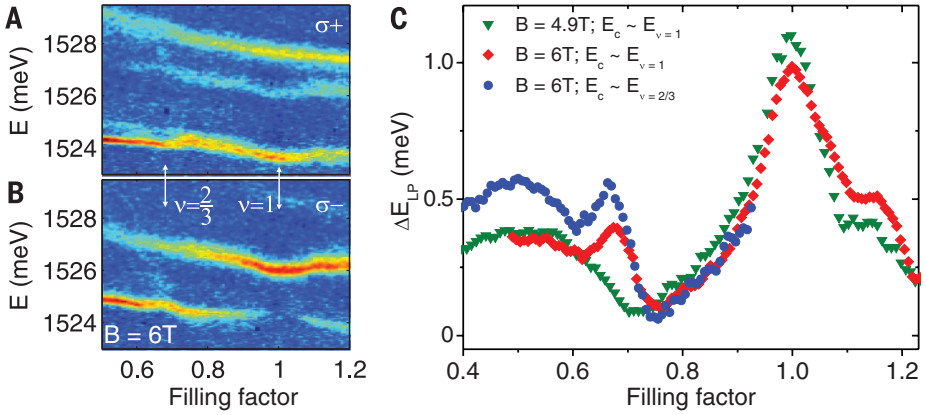

Fig. 4. Fractional QH polariton excitations. (**A** and **B**) Polarization-resolved dR measurements versus V_g performed on sample *B* when the cavity energy is on resonance with the lowest Landau level (B_z = 6 T). The color-code is the same as in Fig. 3. (**C**) The energy difference, $\Delta E_{LP} = E(LP_{\sigma-}) - E(LP_{\sigma+})$, of the σ^- and σ^+ lower polariton branches versus filling factor for different magnetic fields and resonance conditions. Blue circles (B_z = 6 T) correspond to data obtained when the cavity is tuned into resonance with LL0 around ν = 2/3; red squares (B_z = 6 T) and green triangles (B_z = 4.9 T) show data obtained when the cavity is tuned into resonance with LL0 around ν = 1 (data were analyzed from the same scan as in Fig. 3, E and F).

Our B_z = 0 experiments reveal a previously unknown cavity excitation–induced strongly correlated state that requires a new theoretical framework to describe a mobile 2DEG impurity in a cavity-QED setting. Furthermore, $B_z \neq 0$ experiments establish cavity-QED as an invaluable spectroscopic tool for investigating and manipulating properties of many-body states in a 2DEG. By increasing the cavity lifetime, it should be possible to enhance the measurement sensitivity and to observe the incompressibility-induced modification of the polariton splitting. Semi-integrated cavity structures not only allow for a factor of 20 increase in lifetime but also enable tuning the electric-dipole coupling strength (*28*). More intriguing possibilities raised by our observations include observation of nonequilibrium dynamics after an optical quench into a fractional QH state. Last, the system we consider in the B_z = 0 limit could also be viewed as a new nonlinear optical system in which n_e of the 2DEG can be used to change the effective Bohr radius and consequently the strength of polariton-polariton interactions (*29*).

REFERENCES AND NOTES

1. C. Weisbuch, M. Nishioka, A. Ishikawa, Y. Arakawa, *Phys. Rev. Lett.* **69**, 3314–3317 (1992).
2. H. Deng, H. Haug, Y. Yamamoto, *Rev. Mod. Phys.* **82**, 1489–1537 (2010).
3. K. Ohtaka, Y. Tanabe, *Rev. Mod. Phys.* **62**, 929–991 (1990).
4. N. S. Averkiev, M. M. Glazov, *Phys. Rev. B* **76**, 045320 (2007).
5. A. Gabbay, Y. Preezant, E. Cohen, B. M. Ashkinadze, L. N. Pfeiffer, *Phys. Rev. Lett.* **99**, 157402 (2007).
6. M. Baeten, M. Wouters, http://arxiv.org/abs/1404.2048 (2014).
7. B. Sbierski *et al.*, *Phys. Rev. Lett.* **111**, 157402 (2013).
8. S. Das Sarma, A. Pinczuk, Eds., *Perspectives on Quantum Hall Effects* (Wiley, New York, 1996).
9. Materials and methods are available as supplementary materials on *Science* Online.
10. B. R. Bennett, R. A. Soref, J. A. del Alamo, *IEEE J. Quantum Electron.* **26**, 113–122 (1990).
11. P. W. Anderson, *Phys. Rev. Lett.* **18**, 1049–1051 (1967).
12. M. S. Skolnick *et al.*, *Phys. Rev. Lett.* **58**, 2130–2133 (1987).
13. M. Perrin, P. Senellart, A. Lemaître, J. Bloch, *Phys. Rev. B* **72**, 075340 (2005).
14. R. Houdré *et al.*, *Phys. Rev. Lett.* **73**, 2043–2046 (1994).
15. A. Rosch, T. Kopp, *Phys. Rev. Lett.* **75**, 1988–1991 (1995).
16. I. Bar-Joseph, *Semicond. Sci. Technol.* **20**, R29–R39 (2005).
17. P. Plochocka *et al.*, *Phys. Rev. Lett.* **102**, 126806 (2009).
18. L. Tiemann, G. Gamez, N. Kumada, K. Muraki, *Science* **335**, 828–831 (2012).
19. E. H. Aifer, B. B. Goldberg, D. A. Broido, *Phys. Rev. Lett.* **76**, 680–683 (1996).
20. B. I. Halperin, *Hel. Phys. Acta* **56**, 75–102 (1983).
21. J. P. Eisenstein, H. L. Stormer, L. N. Pfeiffer, K. W. West, *Phys. Rev. B* **41**, 7910–7913 (1990).
22. I. V. Kukushkin, K. von Klitzing, K. Eberl, *Phys. Rev. Lett.* **82**, 3665–3668 (1999).
23. J. H. Smet *et al.*, *Nature* **415**, 281–286 (2002).
24. B. Verdene *et al.*, *Nat. Phys.* **3**, 392–396 (2007).
25. J. Hayakawa, K. Muraki, G. Yusa, *Nat. Nanotechnol.* **8**, 31–35 (2013).
26. T. Chakraborty, *Surf. Sci.* **229**, 16–20 (1990).
27. N. Kumada *et al.*, *Phys. Rev. Lett.* **89**, 116802 (2002).
28. B. Besga *et al.*, http://arxiv.org/abs/1312.0819 (2013).
29. I. Carusotto, C. Ciuti, *Rev. Mod. Phys.* **85**, 299–366 (2013).

ACKNOWLEDGMENTS

The authors acknowledge insightful discussions with L. Glazman, M. Goldstein, A. Rosch, A. Srivastava, and J. von Delft. This work is supported by Swiss National Center of Competence in Research Quantum Photonics (NCCR QP), research instrument of the Swiss National Science Foundation (SNSF).

SUPPLEMENTARY MATERIALS

www.sciencemag.org/content/346/6207/332/suppl/DC1
Materials and Methods
Supplementary Text
Figs. S1 to S8
References (*30*–*35*)

10 July 2014; accepted 17 September 2014
Published online 2 October 2014;
10.1126/science.1258595